UNMANNED AIRCRAFT SYSTEM ASSESSMENTS OF LANDSLIDE SAFETY FOR TRANSPORTATION CORRIDORS

FINAL PROJECT REPORT

by

Keith Cunningham
University of Alaska, Fairbanks

Michael J. Olsen, Matt O' Banion
Oregon State University

Joseph Wartman, Claire Rault
University of Washington

Sponsorship: Pactrans

for
Pacific Northwest Transportation Consortium (PacTrans)
USDOT University Transportation Center for Federal Region 10
University of Washington
More Hall 112, Box 352700
Seattle, WA 98195-2700

In cooperation with US Department of Transportation-Research and Innovative Technology Administration (RITA)

Disclaimer

The contents of this report reflect the views of the authors, who are responsible for the facts and the accuracy of the information presented herein. This document is disseminated under the sponsorship of the U.S. Department of Transportation's University Transportation Centers Program, in the interest of information exchange. The Pacific Northwest Transportation Consortium, the U.S. Government and matching sponsor assume no liability for the contents or use thereof.

Technical Report Documentation Page

1. Report No. IE/AUTC/-2016-12	2. Government Accession No.	3. Recipient's Catalog No.

4. Title and Subtitle
Unmanned Aircraft System Assessments of Landslide Safety for Transportation Corridors

5. Report Date
December 2016

6. Performing Organization Code
G10259-339319

7. Author(s)
Keith W. Cunningham – University of Alaska
Michael Olsen – Oregon State University
Joseph Wartman – University of Washington
Matt O'Banion – Oregon State University

8. Performing Organization Report No.
INE/AUTC-2016/12

9. Performing Organization Name and Address
Alaska University Transportation Center
University of Alaska Fairbanks
P.O. Box 755900
Fairbanks, AK 99775-5900

10. Work Unit No. (TRAIS)

11. Contract or Grant No.
DTRT-13-G-UTC40

12. Sponsoring Organization Name and Address
Pacific Northwest Transportation Consortium
University of Washington
More Hall 112, Box 352700
Seattle, WA 98195-2700

13. Type of Report and Period Covered
Final Report

14. Sponsoring Agency Code
UW-BPO-3882

15. Supplementary Notes
Report uploaded at www.pacTrans.org

16. Abstract
An assessment of unmanned aircraft systems (UAS) concluded that current, off-the-shelf UAS aircraft and cameras can be effective for creating the digital surface models used to evaluate rock-slope stability and landslide risk along transportation corridors. The imagery collected with UAS can be processed using a photogrammetry technique called Structure-from-Motion (SfM) which generates a point cloud and surface model, similar to terrestrial laser scanning (TLS). We treated the TLS data as our control, or "truth," because TLS is a mature and well-proven technology. The comparisons of the TLS surfaces and the SFM surfaces were impressive – if not comparable in many cases. Thus, the SfM surface models would be suitable for deriving slope morphology to generate rockfall activity indices (RAI) for landslide assessment. This research also revealed that UAS are a safer alternative to the deployment and operation of TLS operating on a road shoulder because UAS can be launched and recovered from a remote location and capable of imaging without flying directly over the road. However, both the UAS and TLS approaches still require traditional survey control and photo targets to accurately geo-reference their respective digital surface models.

17. Key Words
Research management (Cw), Planning (Ep), Innovation (Ey), Maintenance practices (Fmb), Mathematical analysis (Uh), Geometry (Up), Statistical analysis (Us), Risk (Hk), Risk assessment (Hka), Alaska, Asset management, GIS, Slope stability, Laser scanning, Lidar, Mobile Mapping, Risk-based, Rockfall energy index, Evaluate, Highway

18. Distribution Statement
No restrictions.

19. Security Classification (of this report)	20. Security Classification (of this page)	21. No. of Pages	22. Price
Unclassified.	Unclassified.	65	NA

Form DOT F 1700.7 (8-72) **Reproduction of completed page authorized**

METRIC (SI*) CONVERSION FACTORS

APPROXIMATE CONVERSIONS TO SI UNITS

Symbol	When You Know	Multiply By	To Find	Symbol
		LENGTH		
in	inches	25.4	millimeters	mm
ft	feet	0.3048	meters	m
yd	yards	0.914	meters	m
mi	Miles (statute)	1.61	kilometers	km
		AREA		
in^2	square inches	645.2	millimeters squared	cm^2
ft^2	square feet	0.0929	meters squared	m^2
yd^2	square yards	0.836	meters squared	m^2
mi^2	square miles	2.59	kilometers squared	km^2
ac	acres	0.4046	hectares	ha
		MASS (weight)		
oz	Ounces (avdp)	28.35	grams	g
lb	Pounds (avdp)	0.454	kilograms	kg
T	Short tons (2000 lb)	0.907	megagrams	mg
		VOLUME		
fl oz	fluid ounces (US)	29.57	milliliters	mL
gal	Gallons (liq)	3.785	liters	liters
ft^3	cubic feet	0.0283	meters cubed	m^3
yd^3	cubic yards	0.765	meters cubed	m^3

Note: Volumes greater than 1000 L shall be shown in m^3

		TEMPERATURE (exact)		
°F	Fahrenheit temperature	5/9 (°F-32)	Celsius temperature	°C
		ILLUMINATION		
fc	Foot-candles	10.76	lux	lx
fl	foot-lamberts	3.426	candela/m^2	cd/cm^2
		FORCE and PRESSURE or STRESS		
lbf	pound-force	4.45	newtons	N
psi	pound-force per square inch	6.89	kilopascals	kPa

These factors conform to the requirement of FHWA Order 5190.1A *SI is the symbol for the International System of Measurements

APPROXIMATE CONVERSIONS FROM SI UNITS

Symbol	When You Know	Multiply By	To Find	Symbol
		LENGTH		
mm	millimeters	0.039	inches	in
m	meters	3.28	feet	ft
m	meters	1.09	yards	yd
km	kilometers	0.621	Miles (statute)	mi
		AREA		
mm^2	millimeters squared	0.0016	square inches	in^2 m^2
meters squared		10.764	square feet	ft^2 km^2
kilometers squared		0.39	square miles	mi^2 ha
hectares (10,000 m^2)		2.471	acres	ac
		MASS (weight)		
g	grams	0.0353	Ounces (avdp)	oz
kg	kilograms	2.205	Pounds (avdp)	lb mg
megagrams (1000 kg)		1.103	short tons	T
		VOLUME		
mL	milliliters	0.034	fluid ounces (US)	fl oz
liters	liters	0.264	Gallons (liq)	gal
m^3	meters cubed	35.315	cubic feet	ft^3
m^3	meters cubed	1.308	cubic yards	yd^3

		TEMPERATURE (exact)		
°C	Celsius temperature	9/5 °C+32	Fahrenheit temperature	°F
		ILLUMINATION		
lx	lux	0.0929	foot-candles	fc
cd/cm^2	candela/m^2	0.2919	foot-lamberts	fl
		FORCE and PRESSURE or STRESS		
N	newtons	0.225	pound-force	lbf
kPa	kilopascals	0.145	pound-force per square inch	psi

Table of Contents

List of Figures

List of Abbreviations

AK DOT&PF: Alaska Department of Transportation & Public Facilities

ASCII: American Standard Code for Information Interchange

DEM: Digital Elevation Model

DMI: Distance Measurement Indicator

DSM: Digital Surface Model

DTM: Digital Terrain Model

FHWA: Federal Highway Administration

GAM: Geotechnical Asset Management

GIS: Geographic Information System

GNSS: Global Navigation Satellite System

GPS: Global Positioning System Hz: Hertz

IMU: Inertial Measurement Unit

INS: Inertial Navigation System

KE: Kinetic Energy

KMZ: Zipped KML (Keyhole Markup Language)

Lidar: Light Detection and Ranging

MAP 21: Moving Ahead for Progress in the 21st Century Act

MSE: Mechanically Stabilized Earth

MLS: Mobile Laser Scan or Mobile LiDAR System

MP: Mile Post

NCHRP: National Cooperative Highway Research Program

OLS: Ordinary Least Squares

ODR: Orthogonal Distance Regression

PacTrans: Pacific Northwest Transportation Consortium

PBV: Point Bounding-Box Vertex

RAI: Rockslope Activity Index

RDA: Rockslope Deterioration Assessment

RGB: Red Green Blue

RHRS: Rockfall Hazard Rating System

RINEX: Receiver Independent Exchange

RMS: Root Mean Square RTK: Real Time Kinematic

TAM: Transportation Asset Management

TIN: Triangulated Irregular Network

TLS: Terrestrial Laser Scan or Terrestrial Lidar Scan

TRB: Transportation Research Board

UAS: Unmanned Aircraft System

UTIC: UAS and Terrestrial Imagery Combination

VTOL: Vertical Take Off and Landing

WSDOT: Washington State Department of Transportation

XYZ: Cartesian coordinates with three dimensional, orthogonal axes

XYZRGBI: XYZ coordinates with RGB color values and Intensity value

Acknowledgments

This research grant, DTRT13-G-UTC40, is funded by the Pacific Northwest Transportation Consortium (PacTrans). PacTrans is a consortium of university transportation centers located in Washington, Oregon, Idaho, and Alaska. The lead research agency was the University of Alaska Fairbanks (UAF) with Keith Cunningham serving as Principal Investigator. Co-investigators were Michael Olsen from Oregon State University (OSU) and Joseph Wartman from the University of Washington (UW).

We owe a special thanks to Jeffrey Hollingsworth at the University of Alaska Anchorage (UAA) for assisting with the local survey control network and Rayjan Wilson from the University of Alaska Fairbanks, who assisted with the operation of the unmanned aircraft systems.

A number of students participated in this research. At the University of Washington, a visiting student, Claire Rault, participated in the image collection and processing. Students from Oregon State University who assisted with this project included Matt O' Banion, Alireza Kashani, Martha McAlister, and Patrick Burns.

Finally, we acknowledge and appreciate the support of Leica Geosystems, David Evans and Associates, MicroSurvey Inc., and Maptek I-Site in providing hardware and/or software utilized in this study. Funding for the 3D CAVE was provided by the Eric HI and Janice Hoffman Faculty Scholar program.

Executive Summary

Unmanned aircraft systems (UAS), or drones, are an area of growing research for many fields, including transportation. The advantageous, flexible perspective of the airborne camera can collect detailed, close-range imagery that can be used to understand and evaluate geologic features affecting landslide safety. Simultaneously, a renaissance in close-range photogrammetry is evolving with drone sensors, which enables detailed surface models to be constructed from overlapping images by using structure-from-motion (SfM) algorithms. These digital surface models (DSM) allow further analysis of the morphology of a slope's geology, with resolutions approaching and possibly surpassing traditional terrestrial laser scanning, also known as lidar.

This report describes how an off-the-shelf UAS and camera were used to create detailed DSM files consisting of point clouds and triangulated irregular networks (TIN). It also presents how these UAS SfM data products compare to current and prior lidar data collected at the same sites over the past three years. The sites collected are both in Alaska, one along the Glenn Highway between Palmer and Glennallen (mileposts 78 to 89) and the other on the Parks Highway near the entrance to the Denali National Park (mileposts 239 and 247).

In addition to fundamental research contributions, the project created a technology transfer educational video aimed at state departments of transportation. The video can be viewed at: (https://youtu.be/4LrmLbwbK7Y).

This page is intentionally left blank

Chapter 1 Introduction

Landslides pose significant challenges and life-safety risks for transportation networks. They are a chronic concern for highway managers across the United States, in general, and specifically in the Pacific Northwest. A well-known recent example is the 2014 Oso, Washington, Landslide, which killed 43 people, including at least one motorist on State Route 530 (GEER 2014). In addition to the human losses (and injuries), this event resulted in capital losses of over $150 million and closed a major east-west thoroughfare for several months. Rock-slope failures are a particularly dangerous type of landslide owing to their potentially large volumes, high velocities, long travel distances, and impact forces. Such failures have resulted in fatalities of motorists in each of the Pacific Northwest states. Reflecting the significance of this problem, the U.S. National Research Council recently recommended a 15-fold increase in funding for landslide research (NRC 2003).

The current state-of-the-practice for assessing landslide safety along transportation corridors typically involves qualitative scoring of landslide hazards using simplified classification systems such as the Rockfall Hazard Rating (RHRS, Pierson 1991) or the Slope Mass Rating (SMR). These and other similar systems (e.g., Nicholson 2005) provide a site-specific relative scoring based on field reconnaissance and assessment of rock slopes. While such systems serve as a useful tool for the ranking of slope hazards, their qualitative nature does not directly support the current trend toward performance-based asset management of transportation infrastructure. Moreover, current best practices for management do not readily facilitate proactive slope management – identifying and remediating hazardous conditions before a failure occurs. In part, this disconnect is due to the widespread spatial and temporal distribution of landslides.

Additionally, the traditional methods of measuring and managing slopes is time consuming and costly, not to mention the inherent safety risk present to geotechnical survey crews working on narrow highway shoulders in areas with low traffic visibility.

Historically, slopes have been typically remediated after hazardous events such as landslides or rock falls. Dealing with unstable slopes as they happen does not represent diligent nor proactive ownership of such assets. A proactive approach will likely yield many important safety benefits.

This research develops new, state-of-the-art tools and techniques to enable more efficient and effective safety assessments of unstable highway slopes. The tools used included unmanned aircraft systems (UAS), which provide a safer and superior perspective than terrestrial lidar for the modeling of slopes. We also investigated the generation of surface models from the optical camera carried by the UAS using a recently maturing technique called Structure from Motion (SfM), which uses the motion parallax created from the UAS flight to reconstruct the three-dimensional surface models of the slope being imaged. UAS technology may be a more cost effective method of conducting slope surveys than traditional methods, as well as proving safer for the gathering of geotechnical slope data.

To this end, this research was designed and conducted to evaluate and document the capabilities and limitations of UAS for analyzing slope stability for landslide safety along critical transportation corridors.

The specific research objectives to be addressed included the following:

1. Can UAS efficiently provide information for rock slope stability assessments?
2. Compare digital surface models (DSMs) from UAS to those from terrestrial laser scans (TLS). Key questions are:

a. Does the UAS airborne perspective improve the DSM in comparison to ground-based TLS?
b. How much survey control and geo-referencing is necessary?
c. What magnitude of change can be detected from SfM models?
d. How can UAS SFM models and lidar models complement each other?

3. Can the Rockfall Activity Index (RAI) landslide assessment system be implemented with the UAS DSM?
4. How can UAS be used in other transportation applications?

Chapter 2 Literature Review

This section first describes landslide hazards, followed by a discussion of technologies that were used in this research.

2.1 Landslide Hazards

Landslides hazards have traditionally been analyzed at the site-specific scale. There is, however, growing interest in expanding landslide hazard assessment over substantially larger spatial extents, a sentiment emphasized in the current USGS National Landslide Hazards Mitigation Strategy. In addition to providing efficient and cost-effective landslide safety assessments, regional-scale analysis tools have the potential to capture "system-level" performance and spatial propagation of risk within a defined study area. Such capabilities are important when considering the effects of landslides on geographically distributed critical infrastructure systems, which are highly susceptible to damage from slope failures.

Road cuts through rocky terrain often result in steep rock-slopes, which can be susceptible to rockfall – a process involving detachment, fall, rolling, and/or bouncing of rocks (Hunger et al., 2014). Rockfall is a reoccurring hazard along transportation corridors in mountainous regions throughout North America. Tens of millions of dollars ($US) are spent annually on rock-slope maintenance and mitigation (Turner and Jayaprakas, 2012).

Current methods for characterization of rockfall hazards and risk rely on rockmass classification (e.g., Pantelidis, 2009) or rockfall hazard rating (e.g., Pierson, 2012) systems that depend on manual visual inspection and simplified calculations. These methods are both qualitative in nature (Budetta and Nappi, 2013) and coarse in spatial resolution. Recent advances in lidar (Light Detecting and Ranging) and other techniques such as SfM photogrammetry now allow rock-slopes to be captured as high resolution 3-D point clouds. TLS allows for systematic acquisition of rock-slope 3-D geometry at high, cm-scale spatial

resolutions (Jaboyedoff et al., 2012; Abellan et al., 2014). TLS has been proven as an appropriate method for rock-slope characterization (e.g., Japoyedoff et al. 2012, Abellan et al. 2009, 2010, 2014, Alba et al. 2009, 2010, Kemeney and Turner, 2008, Rabatel et al. 2008, Giradeau-Montaut 2016, Kromer et al. 2015, Gigli and Casagli, 2011), and monitoring (e.g., Lim et al. 2005, 2010, Rosser et al. 2005, 2007, Lato et al. 2009, Olsen et al. 2009, 2015).

In a previous Pactrans- and Alaska DOT-supported project, the research team capitalized on point cloud-derived terrain models in developing the Rockfall Activity Index (RAI), a recently developed morphology-derived, process-based rock-slope assessment system (Dunham 2014).

The RAI system was developed to automatically categorize geo-referenced lidar point clouds, producing a process-based classification mapping that is used to identify zones of rockslope activity and to approximate the annual release of kinetic energy from slopes. The RAI is calculated by the formula RAI = KE*P, where KE is the kinetic energy released from rockslopes (here, KE = 0.5*mass*velocity^2), and P is the annual probability of kinetic energy release. Rockfall volume and fall height (used to determine mass and velocity) are derived from the point cloud through the classification mapping and direct measurement. The variable P, which describes activity rates, can be estimated or determined more precisely on the basis of earlier lidar change detection at the study sites (Dunham 2014).

The classification mapping uses morphological indices to characterize the slope erosional processes (e.g., "active release of small blocks, overhangs, etc.") at the site. The RAI mapping highlights areas (shown in red) that are likely to produce large energy releases. As indicated by the RAI formulation, the hazard mapping also takes into account the height and size of features to more accurately capture the risk posed to motorists.

The RAI system was based on morphological indicators (slope, roughness, and convexity) and change detection based on 5-cm grid spacing. Additionally, it specifically excludes areas that not visible from scanners and cameras located at ground level (this limitation was addressed in this research project with a top-view UAS).

2.2 Unmanned Aircraft Systems Remote Sensing

Unmanned aircraft systems have matured significantly in the past few years and have found an important niche in academic and scientific research. The UAF in particular has led much of this research with a large variety of sensor payloads for diverse science missions (Cunningham et al., 2014).

UAS have several advantages over terrestrial remote sensing and manned aircraft. One is their ability to fly low and slow, collecting large amounts of optical and other data. Close range inspection and collection of high resolution data is another capability enabled with the hover of rotary-winged UAS. Sometimes overlooked is the ability to program the UAS to collect the same types of data with repeatable missions, by programing the autopilot with specific missions. These capabilities were evaluated in this project.

UAS imagery has proved useful for landslide analysis through SfM 3-D image reconstruction and digital image correlation. Researchers have utilized repeat surveys from UAS platforms to quantify landslide displacements of large, slow-moving landslides (Niethammer et al. 2012, Fernandez et al., 2013, Lucieer et al. 2013, Fernandez et al. 2015, Turner et al., 2015).

Others researchers have utilized the imagery for mapping landslide features such as scarps and deposits for small areas (e.g., Al-Rawabdeh et al. 2016). Murphy et al. (2015) utilized UAS to map damages from the 2014 Oso landslide in Washington. Greenwood et al. (2016) utilized UASs to map some rock masses and slides in Nepal after the 2015 earthquake

event. Finally, Manousakis et al. (2016) presented results of utilizing UAS SfM for rockfall hazard analysis of a slope.

One of the most time consuming and sometimes difficult aspects of UAS image acquisition of natural terrain and slopes is the placement and surveying of ground control points (GCPs). Work by Keeney (2016) presents promising results for using an off-the-shelf UAS and SfM to remotely assess landslide events in near real-time by using direct georeferencing techniques. The use of direct georeferencing allows for the omittance of surveyed GCPs.

2.3 Structure from Motion (SfM)

TLS offers advantages in terms of accuracy, repeatability, and reliability; however, challenges such as cost and the common occurrence of occlusions exist. SfM-based image reconstruction has the potential to solve these challenges (Chandler and Buckley, 2016). SfM is a recent and quickly evolving method of reconstructing surface data (X, Y, Z coordinates with R, G, B color information) from a series of still images with significant overlap taken from a variety of vantage points. The overlap in each image is modeled in such a way that the pixels of the same feature can have their coordinates determined using a parallax technique that exploits the motion of the UAS as it flies and collects images. The results are a surface model extracted from the imagery similar to a lidar point cloud that can also be used to drape each image to form an orthomosaic. The point clouds and digital surface models generated with SfM techniques can be dense, perhaps denser than the lidar point clouds generated from terrestrial lidar scans of Glitter Gulch. For a detailed overview of the use of SfM in geomorphological studies, the reader is referred to Eltner et al. (2016). This review paper also discusses the variety of accuracy assessments techniques implemented and results achieved. In terms of accuracy of SfM, Eltner et al. (2016) reported no significant issues that cannot be mitigated by placement of GCPs, camera calibration, or a high number of images. Conversely, Wilkinson et al. (2016) stated that

SfM data sets were found to contain systematic inaccuracies when compared to TLS and in most circumstances an "elaborate" approach is required for SfM to achieve results similar to those of TLS. Co-acquired independent references such as TLS, total station points, or Global Navigation Satellite System (GNSS) check points are required to appropriately quantify the accuracy of SfM-derived 3-D geometry. Factors such as scale of the object/environment being captured, distance of the camera from the imaged object(s), camera calibration, image network geometry, image-matching performance, surface texture and lighting conditions, and GCP characteristics introduce error into SfM-based 3-D reconstructions (Eltner et al. 2016). Since these factors can dramatically vary from study to study, accuracy for a given SfM model cannot be ensured based on results achieved by previous studies.

2.4 Lidar Terrain Mapping

Lidar mapping is a relatively new, versatile technology, and as such, many applications have not been fully developed. Because of its versatility for many uses within transportation, several state DOTs are using mobile lidar as part of transportation asset management programs to achieve performance and safety metrics (Olsen et al. 2013). Lidar technology produces highly detailed 3-D models of the scene around the sensor. Most mobile scan systems collect millions of points per second at accuracies (Root Mean Square [RMS]) on the order of 3-10 cm at spatial resolutions of 5-10 cm on the target surface. Data can typically be acquired at up to 150 meters from the mobile laser scan (MLS) vehicle. In addition to mapping, most scanners concurrently photograph the scene, assigning RGB color values to each scan point. Intensity values (i.e., the strength of the signal degradation) are also measured, providing additional information about the type of reflecting material (e.g., geology, vegetation cover etc.).

Lidar surveying has become increasingly effective for geotechnical and geologic analysis, particularly for slope stability assessments, particularly along highway slopes. Lidar

has also been used to undertake detailed geological assessments of several landslides, enabling improved understanding of the processes and mechanisms contributing to landslide movement (e.g., Jaboyedoff, 2010). Kemeny and Turner (2008) evaluated the use of laser scanning for highway rock slope stability analyses and found that ground-based LiDAR offered several advantages over traditional techniques, including safety, accuracy, access, and analysis speed. Kemeny et al. (2008) used LiDAR to evaluate several rock-fall sites near highways in Utah and Colorado. Turner et al. (2006) discussed processing procedures to use TLS to evaluate the stability of rocky slopes. Olsen et al. (2012) developed an in-situ change detection program to enable immediate geo-referencing and comparison of new scan data to baseline surfaces to determine the distribution and quantity of change. Olsen et al. (2012) used TLS in conjunction with a geotechnical testing investigation to determine soil strength parameters to evaluate surficial slope failures occurring on fill embankment slopes for the US-20 Pioneer Mountain to Eddyville re-alignment project. Additional scans were acquired to determine the dipping plane of larger failures observed on cut slopes.

Multi-temporal data sets acquired using scanning technology enable detailed change analyses through time. This helps geotechnical engineers understand the progressive patterns of failures and discern the influence of environmental conditions that lead to those failures. Comparisons of each 3-D scan survey enable quantification of erosion rates and surface deformation, which can be used to analyze the pattern and propagation of displacements that have taken place over the past seven years.

Previous PacTrans projects completed by the research team (Metzger et al. 2014, Cunningham et al. 2015) developed several important tools to enable faster processing of lidar data to reduce workflow bottlenecks. These include the following:

1. Batch scripts to generate digital elevation models (DEMs) and derivative products such as slope, aspect, roughness, and curvature maps.
2. A robust ground filtering algorithm for steep slopes to minimize time spent in manual editing and improving the quality of the surface.
3. Supporting code to implement the RAI algorithm to produce a high resolution slope safety characterization mapped directly to a point cloud.

Chapter 3 Study Site/Data

This research built on three years of slope stability research in Alaska at Long Lake and Glitter Gulch. A baseline of TLS data has been established to develop landslide forecast models and for the emerging geotechnical discipline of change detection. The two research sites are along critical transportation corridors linking Alaska's interior to Anchorage, its most populous city. The Long Lake site is on the Glenn Highway between Palmer and Glennallen, between mile posts 78 and 89. The Glitter Gulch site is near the entrance to the Denali National Park, at mile post 239 and 247 of the Parks Highway.

Numerous unstable rock slopes throughout Sites A and B (figure 3.1) were surveyed along the Glenn Highway in Alaska using both TLS and SfM techniques. We also used a survey total station to create a control network with survey targets that were then used to geo-reference both the TLS and SfM data sets.

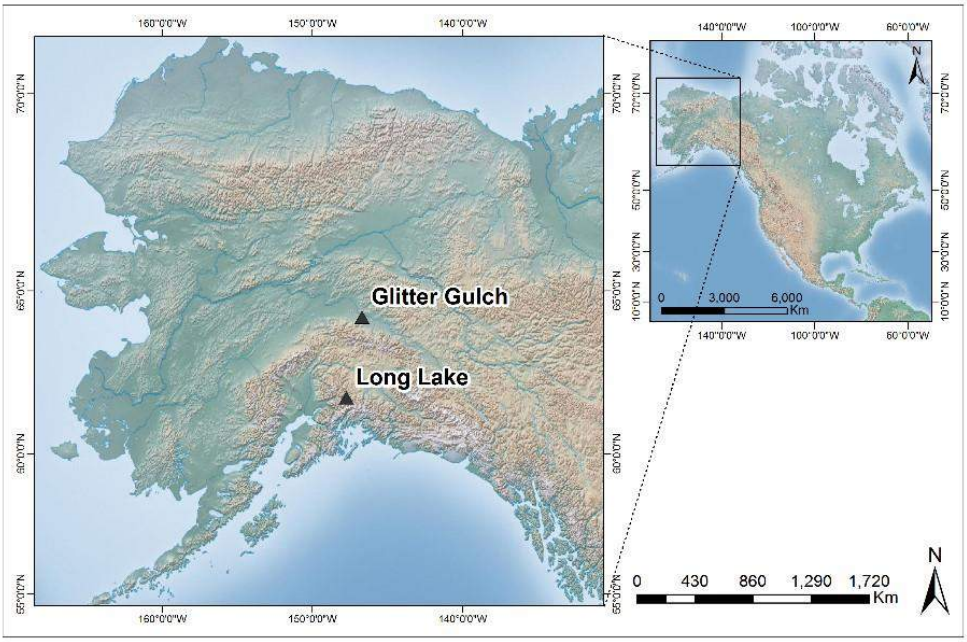

Figure 3.1 - Location of the study sites in Alaska

The Long Lake region primarily comprises sedimentary rocks of the Matanuska and Chickaloon formations. The Matanuska Formation is a marine sedimentary deposit formed during the orogenic rise of the Talkeetna Mountains. The Chickaloon Formation was deposited as propagating alluvial fans on top of the Matanuska Formation that formed as the Talkeetna Mountains were uplifted and sequentially eroded [3]. The highway follows the glacial cut into the Chickaloon Formation; however, no other glacial evidence may be found in the area [4]. Regions of the Matanuska Formation exposed in road cuts along the Glenn Highway largely consist of dark mudstones, and Chickaloon Formation outcrops mainly consist of carbonaceous siltstone, coal, and sandstone [4].

At Glitter Gulch, outside the entrance to the Denali National Park, is an unstable highway slope where several data sets have been collected by the research team. The collection of various types of remote sensing data at this location is being organized and cataloged to generate a remote sensing "super site" for the long-term analysis of the geology and infrastructure. The super site data now include three campaigns of static terrestrial data to model the unstable slope, historic airborne imagery dating to the construction of the road, and "stacks" of synthetic aperture radar data used in the interferometric assessment of slope dynamics for the region. The UAF has acted as the repository of this data archive, which includes other data from research performed with other universities, including an ongoing project with Michigan Technological University.

Chapter 4 Methods

This section describes the procedures for data collection, processing, and analysis. Figure 4.1 presents an overview of the workflow implemented.

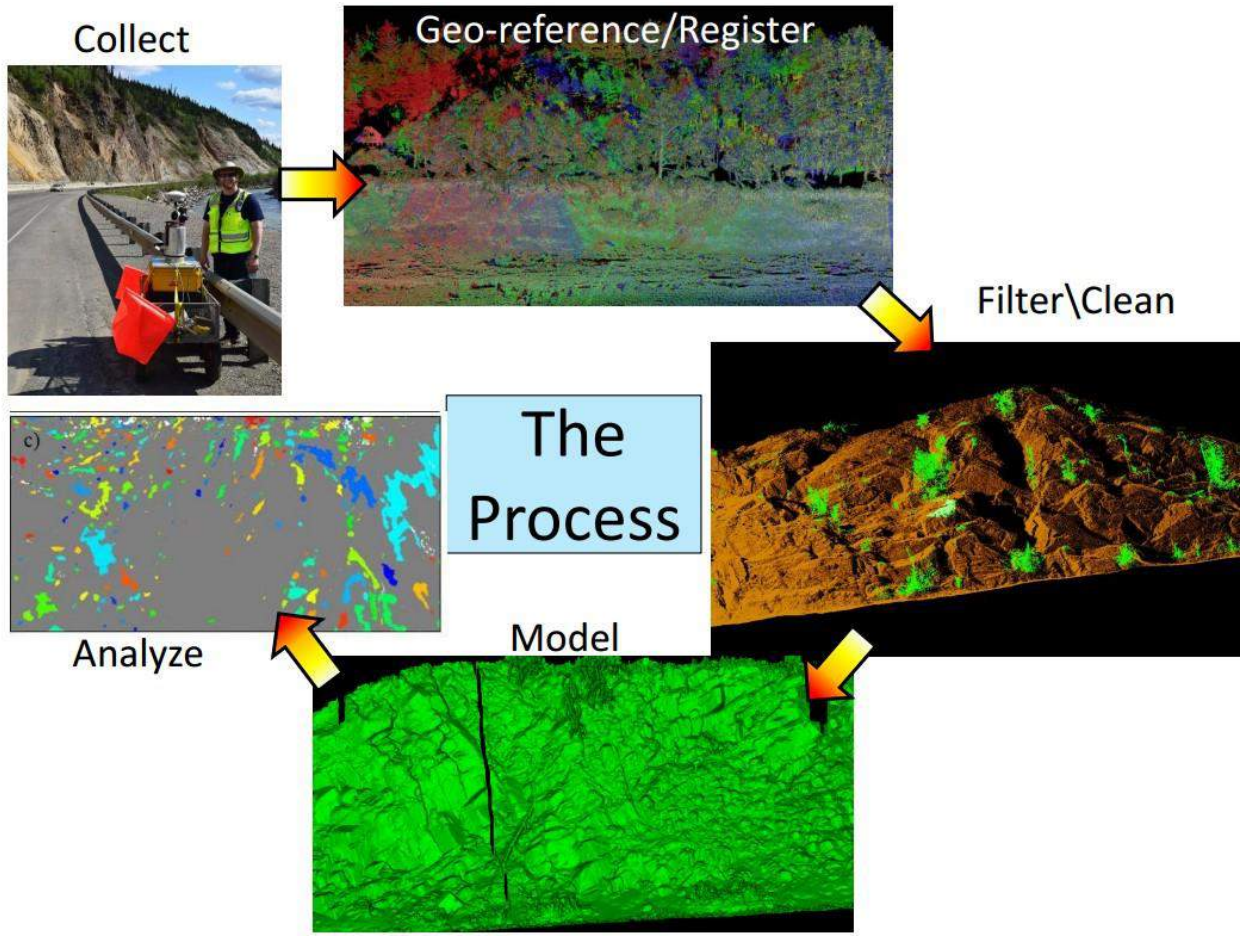

Figure 4.1 - Overview of workflow implemented for this project

4.1 Data Collection

Data were collected at the Glitter Gulch site in May 2015 for 1.5 km of highway and then for several sites in Long Lake (LL71, LL75.8, LL75.9, LL85.5, LL86.9, and LL87) in August 2015. The UAS flights in Glitter Gulch were unsuccessful due to instability of the platform resulting in blurred imagery and therefore were not used for the remaining analysis.

4.1.1 Survey Control

A rigorous survey control network was developed for each study site for accurate georeferencing of both the SfM and TLS data. The survey network was also necessary to scale the SfM data. The control network consisted of both Static and Rapid Static (RS) Global Navigation Satellite System (GNSS) occupations using a Leica GS14 receiver and carefully placed black and white targets to serve as ground control points across the scene. These components of the survey control network were tied together by using a Leica TS15 (1") total station (TS) instrument. Coordinates were established in the Alaska State Plane Coordinate System Zone 4, North American Datum 1983 (2011) Epoch 2010.00, Geoid 12A. The instruments used are shown in figure 4.2.

Figure 4.2 - GNSS receiver and total station used to acquire survey control data

A static GNSS base station was established by using a survey-grade GNSS receiver (Leica GS14) to serve as a reference station for post-processing of short (< 15 min) RS GNSS observations using relative positioning techniques. Its coordinates were established by using the National Geodetic Survey Online Positioning User Service, OPUS (NGS, 2016). Two types of RS GNSS observations were collected in the survey. First, RS control points were positioned along the highway and marked with a survey MAG nail. Second, RS data were acquired at each scan positon by using the scanner mounted receiver.

RS GNSS control points were incorporated into the survey control network by using a TS instrument, prism rod, and 360° degree prism. The center points of all black and white pattern targets within the scene were carefully sighted and acquired by the TS in reflectorless mode. The TS was also used to acquire arbitrary points across the rock slope faces for validation purposes. These rock slope TS points served as an independent reference for evaluating the accuracy of both the SfM and TLS-derived surface models.

The survey targets were each unique to enable the automated registration of their survey positon with their position in both the TLS and SfM point clouds. These targets ensured that the multiple TLS data sets were properly co-registered and that the SfM data were also geo-referenced in the same coordinate system for comparison to the TLS surface. Figure 4.3 shows the survey targets, mounted on clipboards, and placed along the slope for surveying, TLS data collection, and the UAS image collection.

Figure 4.3 - Example of survey targets placed on the slope

4.1.2 TLS Surveys

TLS surveys were performed by using a Reigl VZ-400 laser scanner (figure 4.4) following a stop-and-go scanning approach similar to that presented in Olsen et al. (2009, 2011). The TLS instrument was mounted to a wagon, allowing for efficient mobilization of equipment along the shoulder of the highway. The TLS configuration included a digital SLR camera and survey-grade GNSS receiver mounted on top with known calibrated offsets. Accurate scans could be acquired from an imprecisely levelled wagon platform because of inclination sensors integrated into the TLS instrument (Silvia and Olsen, 2012). Atmospheric conditions, including temperature, pressure, and relative humidity, were entered into the TLS instrument to correct for systematic errors affecting electronic distance measurement capabilities. All scans had a horizontal and vertical field-of-view of 360 and 100 degrees, respectively. The vertical field-of-view was configured as +60 degrees and -40 degrees relative to the horizontal plane. Scans along the highway road cuts were acquired from the side of the road opposite that of the rock

slope and spaced along the road at 40-m to 60-m intervals. Scanning was conducted using an angular sampling resolution of between 0.02 and 0.05 degrees.

Figure 4.4 - TLS survey platform

4.1.3 UAS Imagery

Aerial photographs were obtained by using a DJI Phantom 3 Professional quadcopter UAS platform (Figure 4.5). The Phantom 3 weighed 1.3 kg (including camera payload) and was approximately 40-cm-wide. With its camera payload, the Phantom 3 hds an endurance time of approximately 20 minutes. The UAS platform included an integrated 3-axis gimbal system to stabilize the camera during flight, thus minimizing vibration-induced blur in the aerial images. The gimbal provided a pitch range of -90° (i.e., nadir) to +30°, which could be adjusted in-flight using DJI's mobile flight control application GO. The Phantom 3's integrated camera had a 6.2-

mm x 4.6-mm sensor that produced 12.4-megapixel images. The camera system included a 2-mm (35-mm equivalent) f/2.8 lens. Similar to the terrestrial images, the aerial photographs were shot in bright daylight and recorded in RAW image format. The UAS was flown in the manual mode (i.e., without a pre-programmed flight path) by a pilot positioned within sight of the aircraft at the base of each rock-slope. During the flight, a co-pilot operated the UAS camera by using a remote control system. The UAS was flown at altitudes ranging from approximately 10 m to 30 m above the base of each rock-slope. The aerial platform provided a greater flexibility for positioning the camera system, which allowed us to obtain images from a variety of perspectives, including close-range views (~3 m) of incised and recessed morphological features (e.g., small gorges) and broad-range views (~25) of nearly the entire rock-slope. In general, the aerial photographs were obtained at ~8 m horizontal spacing along lines of fixed altitude. Photographs were taken at downward pitches (-60° to -10°), which allowed us to capture benches and other features that were not visible from ground. The UAS aerial photography required about 40 minutes to complete at each site, including time for at least one landing and re-launch sequence to allow for battery replacement.

Figure 4.5 - Phantom Professional UAS (image courtesy of DJI)

4.1.4 Terrestrial Imagery Acquisition

Supplemental terrestrial photographs were acquired by using a Sony Cyber-shot DSC-RX10 II digital camera with a 24-200 mm (35-mm equivalent) f/2.8 lens. The camera's 13.2 mm by 8.8 mm sensor produces images with a resolution of 20.2 megapixels. Before the fieldwork in Alaska, we performed trial photography campaigns at a benchmarked outdoor test site to determine the optimal camera settings for the SfM work. In our test trials, we obtained the most accurate results when the camera's focal length was fixed at 24 mm and the aperture was set to f/5.6. Adopting these settings, we photographed the rock-slopes in bright ambient daylight (flash was disabled) and recorded the images in RAW format. Although storage intensive, we preferred the RAW image format since it produced minimally processed "digital negatives" whose white balance and color grading could be subsequently adjusted, if necessary. A photographer shot the images in the handheld mode while located within the far road shoulder of a two-lane highway located at the base of the rock-slopes. The camera-to-subject distances varied depending on the width of the shoulder area but were generally in the range of 6 m to 12 m. The photographs were obtained from locations spaced at ~5 m along the base of the rock-slopes, with the aim of having at least 50 percent vertical and horizontal overlap in the neighboring images. In general, single photographs from multiple perspectives were preferred over multiple photographs taken by pivoting from a single location. The terrestrial photography required about an hour to complete at each site.

4.2 Data Processing

4.2.1 Survey Control

The coordinates of the GNSS base station were established by using the static processing available through OPUS. RS GNSS control points were processed against the base station by using GNSS baseline vector processing in Leica Geo Office v.8.3.

At each site, a 3-D, unconstrained, least squares adjustment of the control network was completed by using StarNet 8.0 to produce the final coordinates and uncertainties for the control targets and reflectorless measurements on the cliff surfaces. The following observations were input for the adjustment: ground control point coordinates and associated uncertainties obtained from OPUS and OPUS-RS; GNSS baseline vectors between the base station and rover positions with associated covariance matrices; and the measured distances, horizontal angles, vertical angles, and uncertainties for the total station measurements for each setup. The GNSS baseline vector uncertainties were scaled by a factor of 25 to account for the overly optimistic estimates (sub-mm) obtained during baseline processing. A Chi-square test of goodness of fit was completed and passed at the 5 percent level. Estimated errors of the coordinates for the stations were <1.5 cm (3-D RMS) at the network level and <7mm (3-D RMS) at the local level. Note that these estimates did not include geoid modelling error.

4.2.2 TLS Processing

Post-processing of TLS data was required to merge individual scans into a cohesive point cloud model in a common coordinate system. This process required adjustment of the position and orientation of a given scan location, which resulted in a rigid transformation of the 3-D point cloud acquired from that location. Information derived from the onboard inclination sensors, the top-mounted GNSS receiver, and the relative position of GCP targets captured in the scan allowed for the determination of transformation parameters, including rotations and translations along orthogonal axes.

Prior to performing local registration of the point cloud data, individual scans were leveled in accordance with values reported by the onboard inclination sensors (Silvia and Olsen, 2011). Local registration and geo-referencing of the TLS data were performed in Leica Cyclone v.9.1 software using a weighted least-squares methodology combining target matches and cloud-

to-cloud surface matching constraints. The registered point clouds were subsequently georeferenced to the Alaska State Plane Zone 4 coordinate system by using the adjusted survey control network and the scan position coordinates derived from the top-mounted GNSS receiver.

Quality control of point cloud registrations included review of misalignment error vectors for target constraints, review of total error associated with cloud-to-cloud constraints, and visual inspection of registered point clouds, including cross-section inspection. Anomalous target constraints with 3-D error vectors of greater than 0.025 m were omitted from the registration procedure. Visual inspection of the registered point clouds were performed to identify the presence of any point cloud misalignment artifacts that would require re-registration.

4.2.3 SfM Processing

Initially, three separate SfM models were developed: terrestrial imagery only, UAS imagery only, and a combination of both. However, the combination approach provided the most accurate and reliable reconstruction results, which are described solely herein. These will be referred to as the UAS and Terrestrial Imagery Combination (UTIC) model.

To generate the UTIC model, the following steps were implemented in Agisoft PhotoScan Professional v.1.2.5:

1. The UAS and terrestrial imagery were imported into PhotoScan as one *Chunk.*
2. The "Align Photos" tool was used for initial camera alignment and subsequent development of a sparse 3-D point cloud. Settings used for alignment of photos included: Accuracy = High, Key point limit = 45,000, and Tie point limit = 4,000. For SfM models that included geotagged UAS imagery, the Pair preselection parameter was set to "Reference," otherwise, Pair preselection was set to "Disabled."

3. Following creation of the sparse point cloud, GCP coordinates derived from the survey control network for each site were imported.
4. The “Detect Markers” tool was used to automatically extract the center of any PhotoScan branded targets. The centers of additional non-PhotoScan targets were manually extracted from the imagery.
5. All marker assignments in the source imagery were reviewed to ensure proper extraction of GCP centers and to omit constraints relying on blurry images.
6. Refinement of all GCP markers by using the “Optimize Cameras” tool was performed to recalculate external and internal orientation (including lens distortion parameters) of the camera(s).
7. The “Build Dense Cloud” tool was then used to generate the final high-resolution point cloud. Chosen settings for development of the dense point cloud, included: Quality = High, and Depth filtering = Mild.

4.2.4 Surface Generation

Finalized SfM and TLS point clouds were cropped to include only portions of a given rock slope to be studied. Coarse vegetation removal was performed by manually selecting regions of vegetation in the point cloud for removal. Cropped and cleaned point cloud data were then used to create 5-cm 3-D surface models for each study site, using the methodology presented in [5]. The processed point cloud data generated from TLS and SfM were used to develop 3-D surface models with a resolution of 5 cm. Surface models were created by following the same procedure described in Olsen et al. (2015).

4.3 Quality Evaluation

The SfM quality evaluation focused on the suitability of SfM for the assessment of rock slopes. As such, characteristics including point density, completeness, and the capabilities of SfM to capture surface morphology were evaluated relative to TLS.

4.3.1 Completeness

Completeness was evaluated by generating SfMs from both models and comparing locations with data gaps.

4.3.2 Data Density/Resolution

Point density was determined by sub-sampling the TLS and SfM point clouds with 5 x 5 cm grid cells and recording the number of points in each cell. These were then normalized to units of points per square meter; however, the values are displayed for each 5-cm cell.

4.3.3 Accuracy Assessment

Two independent references were used to assess the accuracy of the SfM-based 3-D reconstructions: co-acquired TLS data and rock slope TS points. Both data sets were tied to the previously discussed survey-grade control network. The TS points acquired across the slope faces were used for evaluating the accuracy of the TLS data as well as geometry derived from SfM.

Maptek I-Site Studio 6.0 software was used to difference the TLS and SfM derived surface models by using the "Color from Distance" tool. A maximum distance threshold of $\pm$ 0.20 m was chosen in order to not include larger discrepancies associated with the presence of inconsistent vegetation. The surface-to-surface distances reported by the Maptek I-Site Studio software represents 3-D distances measured along the normal surface of the base surface. Comparison of the interpolated surface models was chosen instead of a point-to-point evaluation because the accuracy of surface models was more relevant to our preferred unstable rock slope

assessment and monitoring techniques (Dunham, under review). However, point-to-point comparisons were performed by using CloudCompare software (CloudCompare, 2016) and similar results were achieved.

Maptek I-Site Studio was also used to compute the 3-D distances between the discrete rock slope TS points and the point cloud derived surface models. Comparison of the TS points to the TLS surface model served to evaluate the accuracy and precision of the TLS data, ensuring they were appropriate to serve as an independent reference for the evaluation of SfM.

Results of surface-to-surface (TLS to SfM) and point-to-surface (TS points to TLS and SfM) differencing were used to generate statistics including mean distance, standard deviation (σ) of distance, root-mean-squared error (RMSE), and error at 95 percent confidence.

4.3.2 Surface Morphology Analysis

Comparative frequency distribution plots were developed to present the differences in surface morphology captured by TLS and SfM methods. The chosen surface parameters included slope, surface roughness, and a surface morphology-derived rock slope morphological classification, Rock Activity Index (RAI) (Dunham, in review). For surface roughness, both small window (3 x 3) and large window (5 x 5) roughness calculated with standard deviation of slope were used.

4.2.6 Data Visualization

The GeoMat VR system at Oregon State University (figure 4.6) was used for visual quality analysis and verification. This system was constructed on the basis of a hardware configuration and software developed at UC Davis (Low-Cost VR, 2016). GeoMat VR consists of a 65-inch active 3-D LED television coupled with an Optitrack infrared tracking array and VR software (Vrui). The array of three tracking cameras tracks the user's stereoscopic 3-D glasses and a Nintendo Wii remote used for data interaction. When working with high

resolution, complex 3-D point cloud data, an immersive VR system supporting stereoscopic visualization facilitates enhanced data interaction and spatial awareness.

For this study, both TLS and SfM point clouds were added to the same environment, which allowed for direct visual comparison. The color of the SfM cloud was modified to have a red tint so that points derived from SfM could easily be differentiated from those gathered by TLS. This advanced visualization technique enabled detailed inspection of geometric discrepancies between the TLS and SfM data sets.

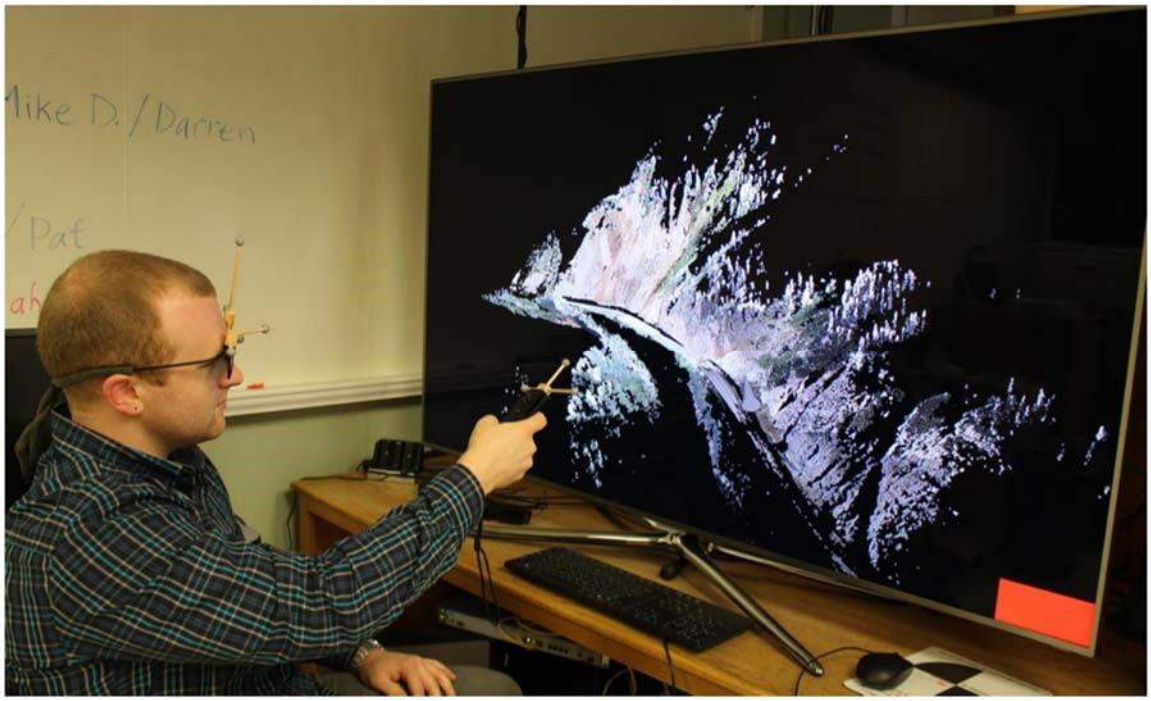

Figure 4.6 - Visualizing the TLS point cloud at Glitter Gulch

Chapter 5 Results

This section presents the results obtained through the analysis of the SfM data. Note that the UAS alone did not provide results as good as those of the UAS Terrestrial Imagery Combination (UTIC) model, which was used for the evaluations.

5.1 UTIC DSM Evaluation

Figure 5.1 shows an example DSM generated by SfM with the combined UAS and terrestrial imagery. Several tests were conducted to evaluate the quality of the DSM. This evaluation was centered on the following aspects:

a) Completeness, in which we evaluated data voids in each
b) Data density, in which we counted the number of points by volume
c) Accuracy comparison of the superimposed models, which looked at deviation of the UAS SfM from the TLS model.

Figure 5.1 - DSM model example from UAS imagery and SfM processing

5.1.1 Completeness evaluation

The flexibility of the UAS enabled it to capture data from difficult areas of the cliff. As can be observed in figure 5.2, both models had data voids, largely due to vegetation blocking the view of the slope. These models were from the Long Lake research site at milepost 71. The TLS model had more data voids, particularly at the top of the slope, than the UAS-generated model. This is an indicator of the scanner "looking" upslope and the surface shape blocking the scanner's laser. However, the UAS-camera obliquely pointed toward the slope, imaging it at an orthogonal angle, did yield a more complete data set. The supplemental terrestrial imagery also helped capture the bottom surface of the overhangs, which was not captured in the UAS imagery.

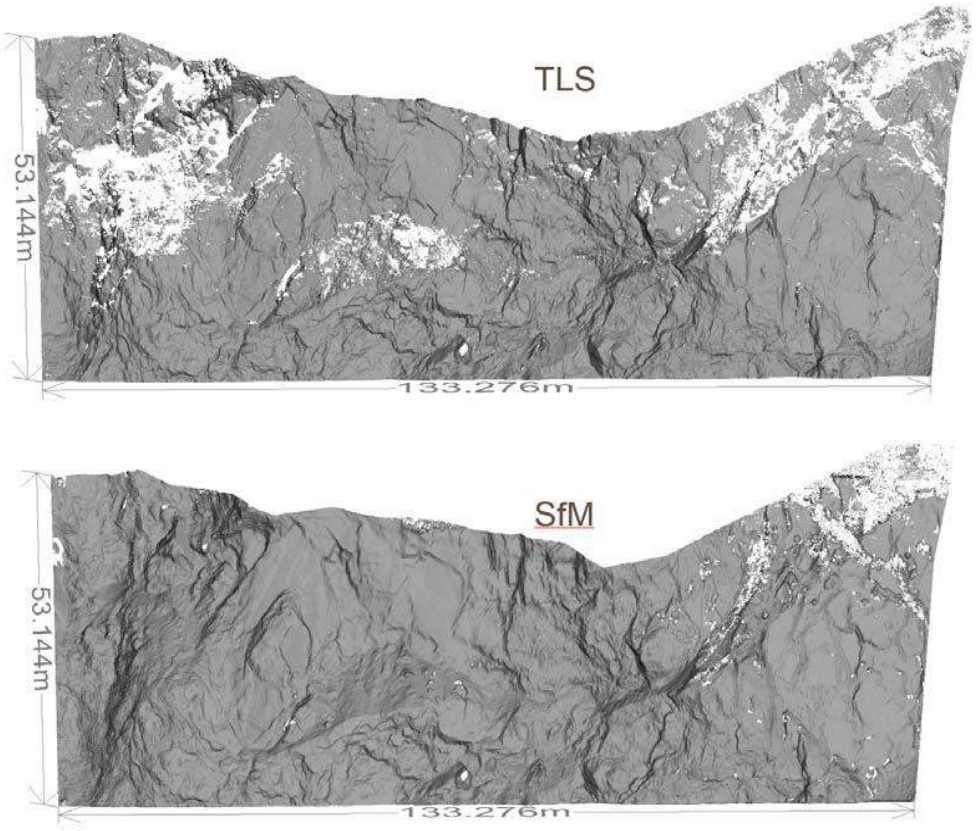

Figure 5.2 - The TLS and SfM surface models, with white patches indicating data voids

5.1.2 Data Density Evaluation

Point densities (figure 5.3) were also quite high with the UTIC SfM data set, with several thousand points per square meter. This density is adequate for determining slope morphologic properties to quantify processes of interest. Note how the UAS SfM data is fairly uniform across the surfaces, whereas the TLS data were denser at the bottom of the slope. This is because the laser scanner was physically closer to the slope along the road, and the scanner was also having to "look up" the slope, resulting in fewer data the further the distance from the scanner, resulting in poorer coverage at the upper sections of the slope.

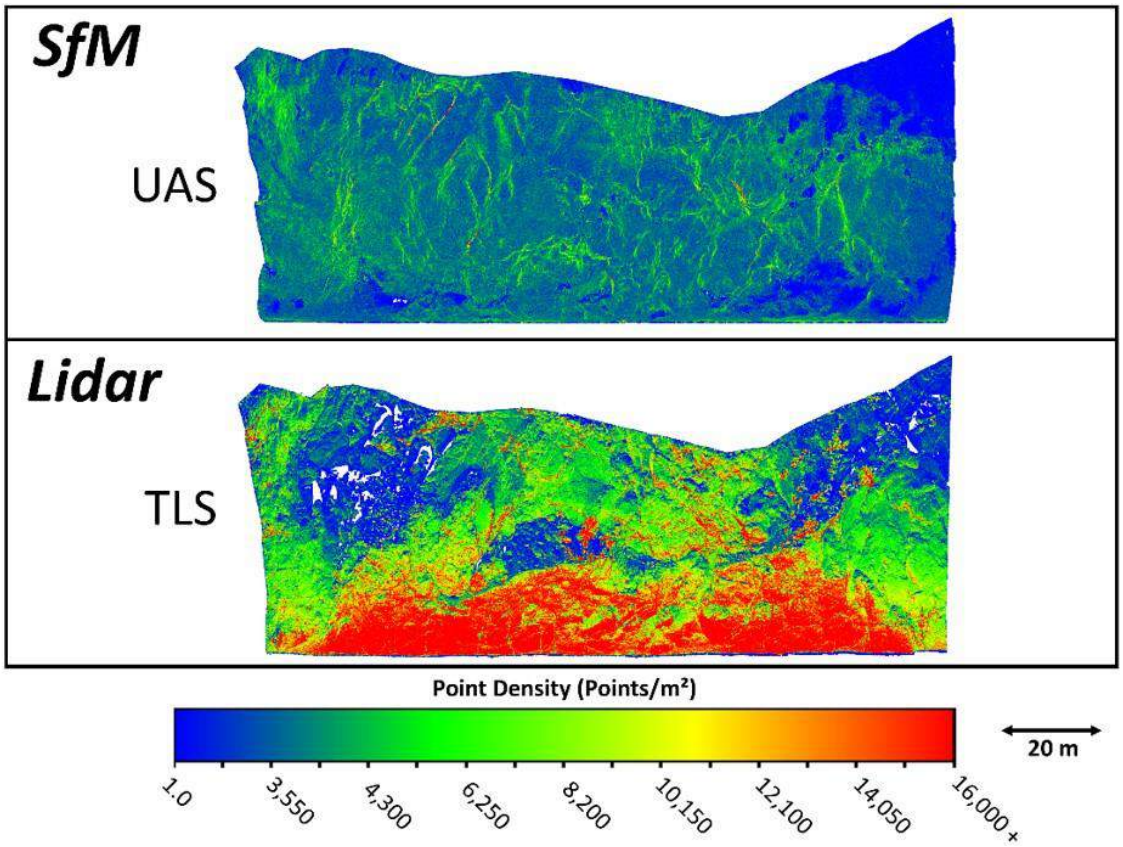

Figure 5.3 - Point densities for both surface models

5.1.3 Accuracy Evaluation

Visual comparison of the TLS to the SfM models and the colored results are shown in figure 5.4 for site LL71. Variation in the two models was on the order of several centimeters. These results were also compared visually by superimposing the two DSMs on top of each other in the VR system. The super-imposition shows that the UAS SfM model floats slightly over the TLS model, by as much as 4 to 8 centimeters throughout the model, and behind the TLS data in other cases. However, a clear pattern of error propagation can be observed upward on the slope as the reconstruction occurs farther from the locales where the ground control targets were placed.

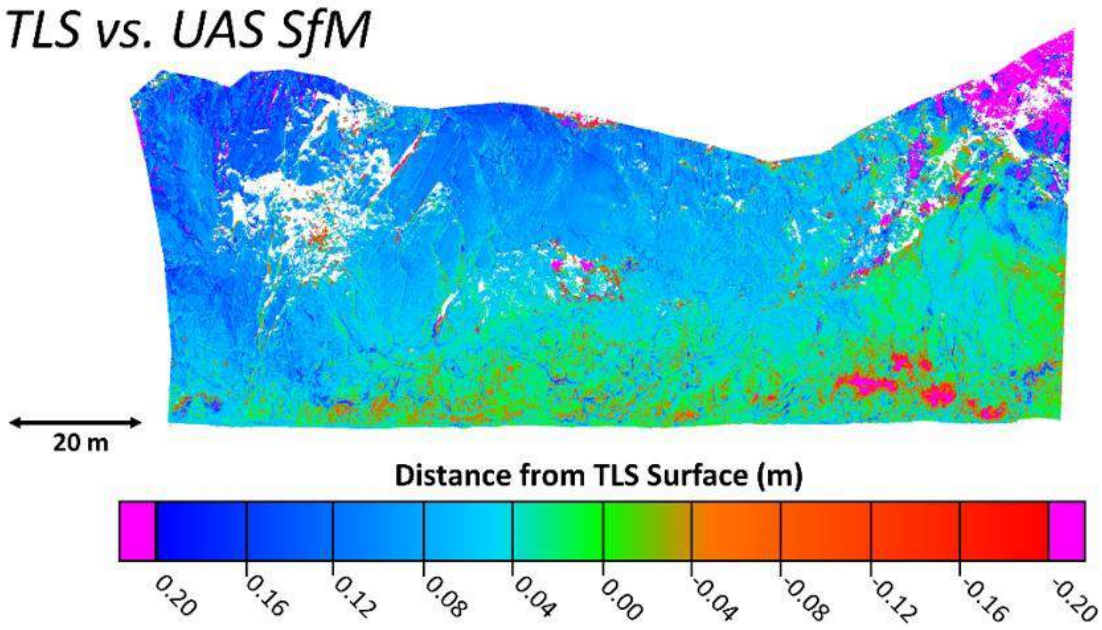

Figure 5.4 – Differences between the SfM and TLS models

A more rigorous statistical analysis of the two surface models yielded the distribution shown in figure 5.5.

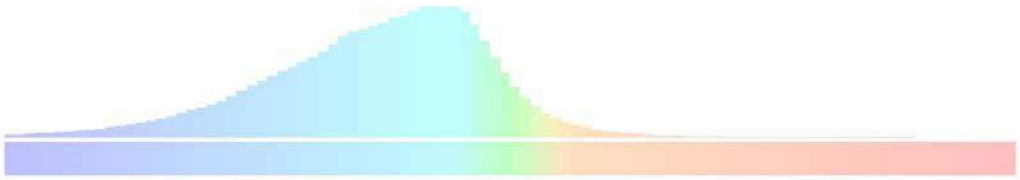

Mean Δ (m)	σ (m)	RMS (m)	95% Conf. (m)	Total Points	Difference Range (± m)	Points in Range	% of Pts in Front of TLS	% of Pts Behind TLS
-0.051	0.046	0.069	0.112	2,577,399	0.20	2,496,275	94.13	5.86

Figure 5.5 - Statistics differentiating the two DSM

Additional comparison of the SfM model with the individual points collected with the survey total station yielded a result similar to that from the comparison with the TLS. This distribution and analysis is shown in figure 5.6. Note the similarity to the results observed from the comparison with the TLS data in figure 5.5.

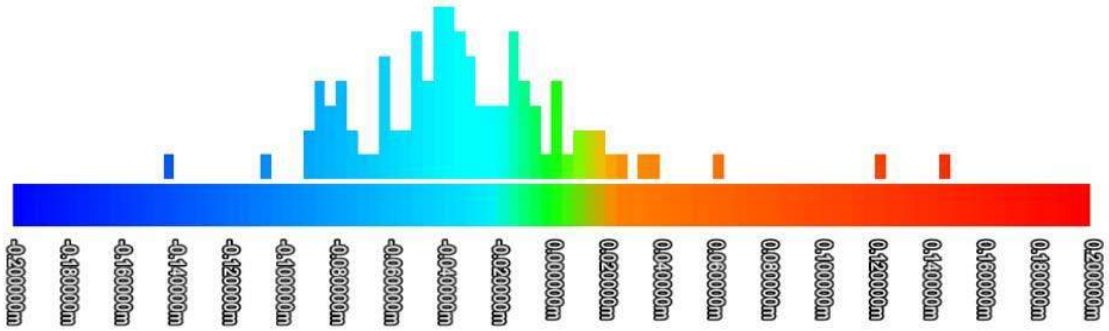

LL71 - UAS				
SITE	Mean Δ (m)	σ (m)	RMS (m)	95% Conf. (m)
LL71 - UAS	-0.032	0.041	0.052	0.084

Figure 5.6 - Statistics from the UTIC SfM surface model

5.2 Geomorphological Evaluation

The point cloud and surface models derived from both the TLS and UAS/SfM approach are comparable, and both are suitable as input data for understanding slope morphology and rockfall activity. Figure 5.7 compares the results of the SfM model with those from the lidar for determining RAI classifications. The Rockfall Activity Indices (RAI) developed over the past three years and the change-detection methods are highly automated for measuring erosional and mass wasting rates (Olsen et al., 2015).

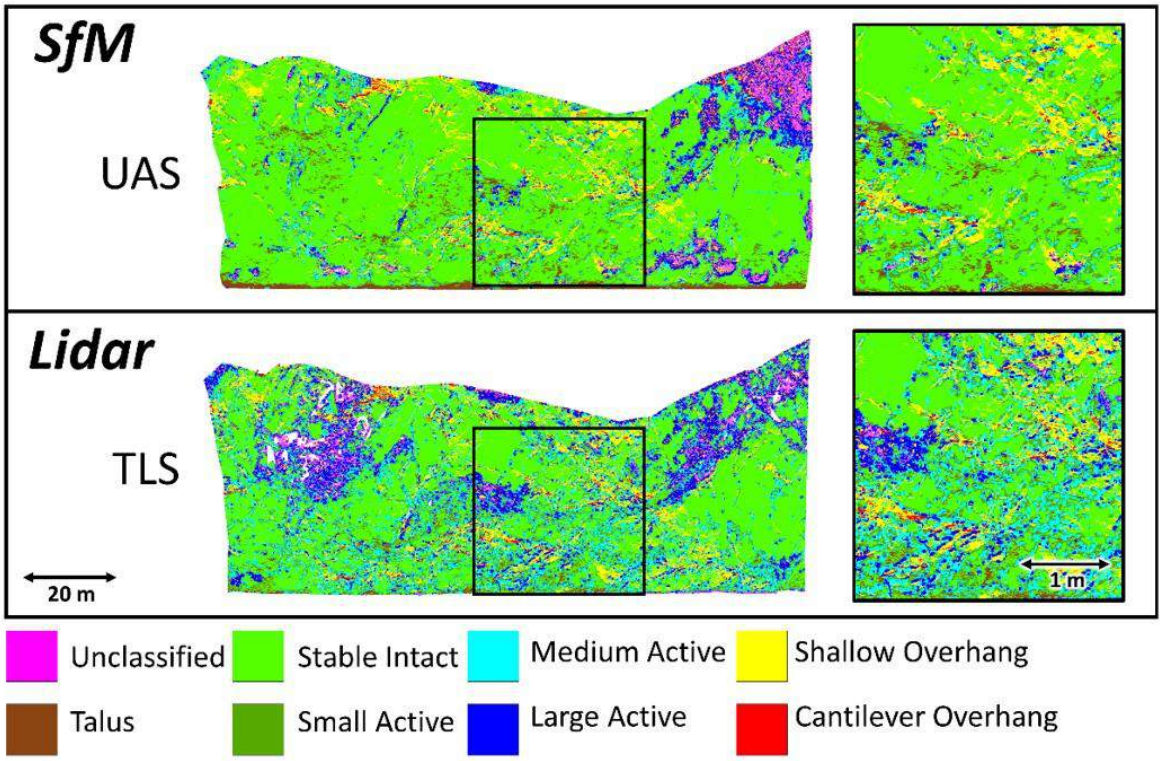

Figure 5.7 - Comparison of slope morphology and rockfall activity from the two DSM

Holistic comparison of the TLS and SfM DSM properties using histograms indicated general agreement (figures 5.8 and 5.9). The overall trend of the plotted properties, including slope, roughness, and Rock Activity Index (RAI) classification, were similar for both sites, with

slight deviations in mean and standard deviation. In most cases, the SfM-derived surface had higher mean and standard deviations than the TLS surface.

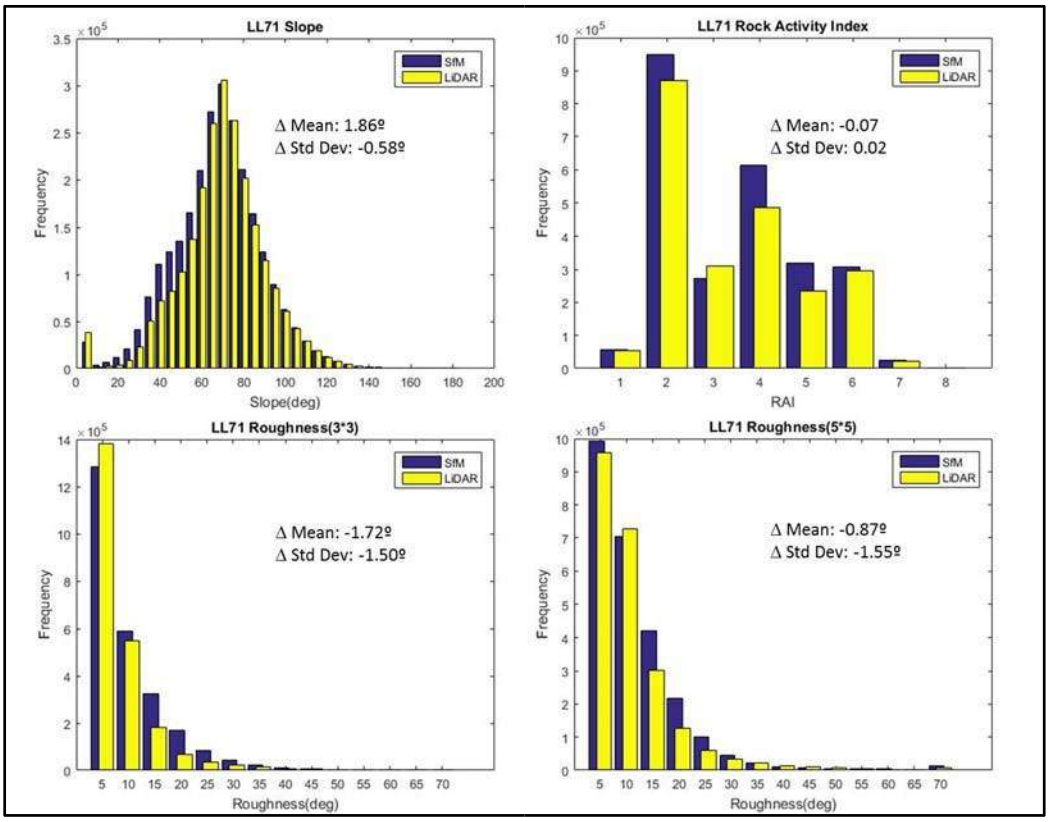

Figure 5.8 - Site LL71 histogram comparison of DSM properties

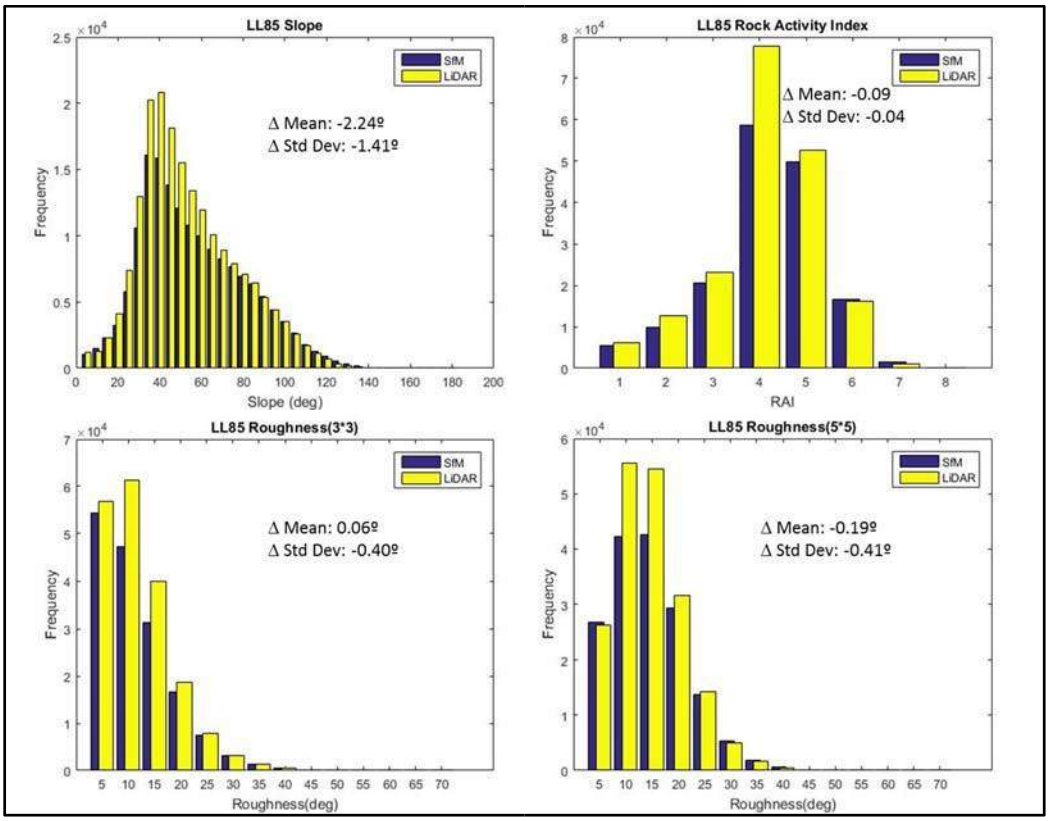

Figure 5.9 - Site LL85.5 histogram comparison of DSM properties

Chapter 6 Discussion

Terrestrial lidar scanning (TLS) is a proven and mature technology for the creation of DSM slopes. The DSMs created are quite accurate, and the number of points in the cloud and surface are huge, typically measured as tens-of-thousands per square meter of surface. The proven accuracy of TLS is the reason that we used the technology for several years of previous research. This same tool was used to evaluate the accuracy and completeness of the UAS/SfM models.

Results indicated that SfM reconstruction is a viable option for unstable rock slope characterization when tied to rigorous survey control. However, some concerning artifacts, over smoothing, and inconsistencies were observed in the SfM-derived models, which caused us to question its suitability for reliably detecting small changes of a few centimeters on unstable rock slopes.

6.1 Evaluation of UAS Efficiencies

The ability of UAS to collect data, especially imagery, from advantageous perspectives makes them an optimal research tool for close-range imaging and digital surface modeling of steep slopes. Gimbaled cameras permit orthogonal pointing and imaging of slopes, no matter how steep. This perspective ensures that the entire slope can be imaged, with no shadows or occlusions created by rock overhangs, including above and below the overhangs. Highly vegetated slopes, however, still pose a significant challenge to UAS SfM data, which cannot capture bare earth as well as active lidar sensors. The effect of vegetation on the DEM can somewhat be mitigated by imaging the slope from multiple look angles to improve capture of the bare earth and rock under the vegetation. However, in areas of dense vegetation, SfM will be unable to produce a DEM.

The UAS evaluated is capable of vertical take-off and landing (VTOL). Therefore, it can be launched and recovered close to the study site, but also at a safe distance and location from vehicular traffic in the transportation corridor. This minimizes risk to both the UAS operators and the traveling public. This provides a significant advantage over TLS, which requires a stable position to set up the instrument. In areas of steep slopes, there is often very limited shoulder width available.

The flight time for battery-operated VTOL UAS is limited to approximately 20 minutes. Fixed wing UAS have longer flight endurance, but they require larger areas for launch and recovery than were available at our study sites. The 20-minute endurance for launch, ferry to the slope in question, and then return is a fairly short distance, which ensures that the UAS pilot is always in visual control of the aircraft and that the radio link to the aircraft is within direct line of sight.

An important aspect to our UAS evaluation was its rapid set-up and quick deployment. The UAS utilized had a simple set-up of approximately 15 minutes, all from a safe location at a distance from passing vehicles. In comparison, the set-up and tear-down of the TLS utilized over the past three years required about 45 minutes, typically within a wide shoulder or on a road. The TLS rig is also substantial and includes a garden cart with a car battery and a heavy aluminum plate to which all the sensors are mounted.

Processing-wise, the SfM software is highly automated but time consuming. Considering the number of images being processed (100's) and their individual size (10's of megabytes), the computer time can take several days of processing. SfM data processing is a "big data" problem that is currently solved with parallel computation and cloud computing, which we experimented with in this research. We utilized both the Amazon Cloud web service as well as a custom server to generate the SfM models efficiently.

6.2 DSM Quality and Completeness

The ability of UAS to collect data, especially imagery, from advantageous perspectives makes them an optimal research tool for close-range imaging and digital surface modeling of steep slopes. Gimbaled cameras permit orthogonal pointing and imaging of slopes, no matter how steep. This perspective ensures that the entire slope can be imaged, with no shadows or occlusions created by rock overhangs, including above and below the overhangs. However, the effect of vegetation must be mitigated by imaging the slope from multiple look angles, ensuring that the bare earth and rock under the vegetation can be rendered as part of a complete digital surface model.

In contrast, each TLS set-up creates a perspective that causes some surface features to not be scanned because of blocked lines of sight. A subsequent survey location may fill in the missing scan data, but all of the scan files from multiple locations must be co-registered to generate a single DSM. A consequence of TLS scanning is the occasional data voids or shadows created by the slope's geomorphology in hard-to-reach locales at the top of the slope.

Finally, the SfM technique with the UAS imaging and the camera pointed orthogonal to the slope surface helps to generate surprisingly complete and reasonably accurate surface models.

6.3 Safety and Operational Considerations

One drawback with linear TLS surveys, especially for slopes and cliffs, such as along a road, are the numerous discreet instrument set-ups. Figure 4.2 shows the TLS rig mounted on a garden wagon with all of its supporting gear. The entire kit includes the lidar scanner, a Global Navigation Satellite System (GNSS), panoramic camera, inclinometers, field computer, and all of this powered from a 12-V car battery.

Another drawback is the need to position the wagon-rig along the road shoulder, which requires a lane-closure permit, highway signage, and sometimes flaggers. This administrative overhead and the inherent safety issues of working with active traffic create risk that can be mitigated with the UAS. The TLS is then wheeled to a survey location, where it is then stationary for about 20 minutes before it is moved again along the shoulder about 50 meters to the next scan location. (Note that for the previous studies we utilized Rapid Static GNSS to position the scanner rather than RTK GNSS, given limitations in line of sight to a base station in the canyon corridors. However, if RTK GNSS or RTN GNSS were available and utilized, the occupation time could be reduced to 5 minutes per set-up location). This process of moving and leaving the stationary TLS on narrow shoulders is a safety issue to the survey team, even with lane closure permits, signage, flaggers, and safety protocols followed.

A more significant conclusion from this research project is how UAS can be effectively used to quickly collect needed data and to do it without a cumbersome TLS survey platform on narrow road shoulders. With further development of the technique, it may be possible to reduce the need for lane closure permits and flaggers associated with traditional surveys. UAS launch and recovery well away from highways and spectators will contribute to safety of operations. Also, the ability of the UAS to fly in parallel with the road and slope, yet stand away some distance from vehicular traffic below, is another safety improvement.

All of these advantages deserve further evaluation and consideration by state departments of transportation to gain acceptance. However, it is also important to note that in order to achieve the highly accurate results sufficient for slope morphology studies, on-the-ground surveying and terrestrial imagery capture are still necessary.

Chapter 7 Conclusions and Recommendations

The following primary conclusions were derived from this research:

1. Rigorous survey ground control is ***imperative*** to obtain satisfactory results in slope modeling from UAS imagery.
2. The UAS provide a more flexible platform than does TLS to improve coverage of the slope.
3. The point cloud data derived through SfM data satisfactorily describe slope morphology.
4. The SfM point cloud was able to satisfactorily perform as an input for RAI classification.
5. The UAS imagery alone was not sufficient for an adequate model and required the addition of terrestrial imagery to obtain results.
6. The UAS provided significant safety and operational benefits over laser scanning. However, it is also important to note that in order to achieve the highly accurate results sufficient for slope morphology studies, on-the-ground surveying and terrestrial imagery capture are still necessary, which still pose some safety concerns.
7. The use of SfM in conjunction with TLS is advantageous and warrants further exploration.

The work completed herein will assist planners/ managers in transportation agencies (and others) to make informed decisions regarding resource allocation with respect to rock slopes. The research provides new tools for objectively identifying which rock slopes pose the greatest risk to a transportation corridor and the customers who use it – thereby indicating where limited resources may have the greatest benefit to a highway corridor and the transportation system as a whole. Proactive slope remediation allows for a cost-effective approach, but more importantly, is a means to mitigate life-safety concerns posed by slope failures. Thus, the public, as both user and taxpayer, will benefit from this project.

7.1 Technology Transfer

The project also provided knowledge and tools that will aid transportation personnel in utilizing advanced technologies in their workflows, particularly for safety analysis. Because of the constantly evolving nature of these technologies, opportunities and resources for training are scarce and expensive. UAS SfM technology provides low cost, easy to implement tools that shatter these barriers. Several mechanisms of technology transfer were implemented, including publications, presentations, and multi-media products.

7.1.1 Publications

The following papers were been published or submitted during the course of this project. Additional publications are in preparation:

Olsen, M., Wartman, J., McAlister, M., Mahmoubadi, H., O'Banion, M., Dunham, L., and Cunningham, K. To Fill or Not to Fill: Sensitivity Analysis of the Influence of Resolution and Hole Filling on Point Cloud Surface Modeling and Individual Rockfall Event Detection. Remote Sensing. 7, 2015, 12103-12134

Lisa Dunham, Joseph Wartman, Michael Olsen, Matthew O'Banion, Keith Cunningham. Rockfall Activity Index (RAI): A Lidar-Derived, Morphology-Based Method for Hazard Assessment. Engineering Geology – Under Review

Matt S. O'Banion, Michael J. Olsen, Claire Rault, Joseph Wartman, Keith Cunningham. Suitability of Structure from Motion for Rock Slope Assessment. In preparation, to submit to IEEE Transactions in Geosciences and Remote Sensing.

7.1.2 Presentations

The following presentations were also given at various conferences and venues:

O'Banion, M.S., Olsen, M.J., Rault, C., Wartman, J., and Cunningham, K. (2016). "Comparison of terrestrial laser scanning and structure from motion techniques for assessment of unstable rock slopes in Alaska," Geological Society of America Abstracts with Programs. Vol. 48, No. 7. doi: 10.1130/abs/2016AM-287069

Olsen, M.J., O'Banion, M., Wartman J., and Cunningham, K. (2016). Efficient georeferencing and analysis of terrestrial laser scanning data for slope stability assessments, International Association of Geodesy (IAG) Commission 4 Symposium, Wroclaw Poland, September 4-7, 2016.

Matt S. O'Banion, Michael J. Olsen, Claire Rault, Joseph Wartman, Keith Cunningham. PacTrans Annual Regional Transportation Conference. *Comparison of Terrestrial Laser Scanning and Structure from Motion Techniques for Assessment of Unstable Rock Slopes in Alaska* (poster). Seattle, WA, 2016

Matt S. O'Banion, Michael J. Olsen, Claire Rault, Joseph Wartman, Keith Cunningham. UAS Mapping 2016. *Comparison of Terrestrial Laser Scanning and Structure from Motion Techniques for Assessment of Unstable Rock Slopes in Alaska.* Palm Springs, CA, 2016 (Invited Talk)

Transportation Research Board (TRB) AFB80 Summer Meeting on Geospatial Data Acquisition Technologies in Design and Construction. *Assessment of Unstable Rock Slopes in Alaska* and *Virtual Reality Based Site Visibility Evaluation.* Corvallis, OR, 2016

O'Banion, M., and Allahyari, M. *3D Capture of Unstable Rock Slopes* (poster). Oregon State University Graduate Research Expo. Portland, OR, 2016

Olsen, M.J., and Wartman J. Rock slope characterization in Alaska using lidar and sfm. Presentation at GNS Science, Wellington, New Zealand, Nov. 5, 2015.

Rault, C. Rock slope characterization in Alaska using lidar and sfm. Poster Presentation, Pactrans Annual Meeting, Fall 2015

Cunningham, K., American Society of Photogrammetry and Remote Sensing Annual Meeting, Keynote Address, Spring 2016

7.1.3 Multi-Media Outreach

In addition to fundamental research contributions, the project created a technology transfer educational video aimed at state departments of transportation (https://youtu.be/4LrmLbwbK7Y).

7.2 Integration of UAS and TLS Data

Both methods can be used to augment any deficiencies in the other model. For example, the data voids from the TLS collection could be filled with point data from the SfM. Likewise, additional match points could be extracted from the TLS data to provide improved and more distributed control points to improve the SfM reconstruction accuracy. However, the precise approach for conducting this process has not yet been evaluated.

References

Abellan et al. 2009, 2010, 2014

Alba et al. 2009, 2010

Al-Rawabdeh, A., He, F., Moussa, A., El-Sheimy, N., Habib, A. (2016). Using an Unmanned Aerial Vehicle-Based Digital Imaging System to Derive a 3D Point Cloud for Landslide Scarp Recognition. Remote Sensing. 8, 95. DOI:10.3390/rs8020095.

Badger, T.C. and Lowell, S. 1992. Rockfall Control Washington State. In Rockfall Prediction and Control and Landslide Case Histories, Transportation Research Record, National Research Council, Washington, No 1342, 14-19.

Belowich, M., "Matanuska Coal Field. Field Guide, Anchorage Alaska," Alaska Geological Society, 2006.

Budetta and Nappi, 2013

Chandler and Buckley, 2016

CloudCompare (version 2.7.0) [GPL software]. (2016) Retrieved from http://cloudcompare.org/

Cunningham, K., Hatfield, M., and Philemonoff, R. "Unmanned Aircraft Systems in Alaska Civil Research," Offshore Technology Conference, 2014.

Cunningham, K., Olsen, M., Wartman, J., Dunham, L., and Stuedlein, A. 2015. A Platform for Proactive Risk-Based Slope Asset Management – Phase II. PacTrans Final Report

Dunham, L. (2014) "Rock-slope activity index (RAI): A Lidar-derived process based rock-slope assessment system," M.S. thesis, Univ. of Washington.

Dunham, L., Wartman, J., Olsen, M.J., O'Banion, M.S*, & Cunningham, K. (Under Review). "Rockfall Activity Index (RAI): A Lidar-derived, morphology-based hazard assessment system," Engineering Geology.

Eltner, A., A. Kaiser, C. Castillo, G. Rock, F. Neugirg, and A. Abellán, "Image-based surface reconstruction in geomorphometry - merits, limits and developments," *Earth Surf. Dyn.*, vol. 4, no. 2, pp. 359–389, May 2016.

Fassi, F., L. Fregonese, S. Ackermann, and V. D. Troia, "COMPARISON BETWEEN LASER SCANNING AND AUTOMATED 3D MODELLING TECHNIQUES TO RECONSTRUCT COMPLEX AND EXTENSIVE CULTURAL HERITAGE AREAS," *ISPRS - Int. Arch. Photogramm. Remote Sens. Spat. Inf. Sci.*, vol. XL-5-W1, pp. 73–80, Feb. 2013.

Fernandez, T., Perez, J.L., Cardenal, F.J., Lopez, A., Gomez, J.M., Colomo, C., Delgado, J., Sanchez, M. (2015) Use of a Light UAV and Photogrammetric Techniques to Study the

Evolution of a Landslide in Jaen (Southern Spain). ISPRS – Int. Arch. Photogramm. Rem. Sens., XL-3/W3, 241-248, DOI:10.5194/isprsarchives-XL-3-W3-241-2015.

Fernandez, T., Perez, J.L., Cardenal, J., Gomez, J.M., Colomo, C., Delgado, J. (2013). Analysis of Landslide Evolution Affecting Olive Groves Using UAV and Photogrammetric Techniques. Remote Sensing. 8, 837. DOI:10.3390/rs8100837.

GEER 2014

Gigli and Casagli, 2011

Giradeau-Montaut 2016

Greenwood, W., Zekkos, D., Lynch J., Bateman, J., Clark, M.K., Chamlagain, D. (2016). UAVBased 3-D Characterization of Rock Masses and Rock Slides in Nepal. 50th US Rock Mechanics/Geomechanics Symposium, Houstion, Texas, 26-29 June 2016.

Hunger et al., 2014

Japoyedoff et al. 2012

Jaboyedoff, M., Oppikofer, T, Abellan, A., Derron, M.H., Loye, A., Metzger, R., Pedrazzini, A., 2010."Use of LiDAR in landslide investigations: a review," Natural Hazards.

Keeney, J.T., (2016). "Using Unmanned Aerial Systems (UAS) and Photogrammetry to Remotely Assess Landslide Events in Near Real-Time". M.S. Thesis, University of Kentucky.

Kemeny, J., and Turner, A.K., (2008) "Ground-based LiDAR Rock slope mapping and assessment," Publication No. FHWA-CFL/TD-08-006.

Kemeny, J., Norton, B., Handy, J., and Donovan, J. (2008). "Three-dimensional digital imaging for the identification, evaluation and management of unstable highway slopes," Final Report for Highway IDEA project 119, TRB NAS.

Kromer et al. 2015

Lato et al. 2009

Lim et al. 2005, 2010

Lucieer, A., de Jong, S., Turner, D. (2013). Mapping landslide displacements using Structure from Motion (SfM) and image correlation of multi-temporal UAV photography. Prog. Phys. Geog. 38, 1-20, DOI:10.1177/03091333135115293.

Low-Cost VR (2016). "Low-Cost VR" http://idav.ucdavis.edu/~okreylos/ResDev/LowCostVR/index.html (Dec. 15, 2016)

Manousakis, J., Zekkos, D., Saroglou, H., Clark, M. (2016). Comparison of UAV-Enabled Photogrammetry-Based 3D Point Clouds and Interpolated DSMs of Sloping Terrain for Rockfall Hazard Analysis. 11th 3D Geoinfo Conference, Athens, Greece, 20-21 October 2016

Metzger, A., Cunningham, K., Olsen, M., Wartman, J., Dunham, L., and Stuedlein, A. 2014. A Platform for Proactive Risk-Based Slope Asset Management – Phase I. PacTrans Final Report

Murphy, R.R., Duncan, B.A., Collins, T., Kendricks, J., Lohman, P., Palmer, T., Sanborn, F. (2015) Use of a small unmanned aerial system for the SR-530 mudslide incident near Oso, Washington. J. of Field Robotics. DOI: 10.1002/rob.21586.

NGS (2016). "OPUS: the Online Positioning User Service, process your GNSS data in the National Spatial Reference System." [Online]. Available: https://www.ngs.noaa.gov/OPUS/. [Accessed: 17-Nov-2016].

Nicolson, D. T. 2005. Hazard assessment for progressive, weathering-related breakdown of excavated rockslopes. Quarterly Journal of Engineering Geology and Hydrogeology, 37, 327–346.

Niethammer, U., James, M.R., Rothmund, S., Travelletti, J., Joswig, M. (2012). UAV-based remote sensing of the Super-Sauze landslide: evaluation and results. Engineering Geology. 128: 2-11.

NRC (2003) Partnerships for Reducing Landslide Risk, National Academies Press, Washington, DC.

Olsen, M.J., Butcher, S., and Silvia, E.P., (2012). Real-time change and damage detection of landslides and other earth movements threatening public infrastructure, OTREC Final Report 2011-22 and ODOT Final Report RS 500-500, 80p.

Olsen, M.J., Wartman, J., McAlister, M., Mahmoudabadhi, H., O'Banion, M.S., Dunham, L., and Cunningham, K., (2015). "To fill or not to fill: Sensitivity analysis of the influence of resolution and hole filling on point cloud surface modeling and individual rockfall event detection." Remote Sensing, Special Issue- Use of lidar and 3D point clouds in geohazards, 79(9),12103-12134. doi:10.3390/rs70912103

Olsen, M.J., Johnstone, E., Kuester, F., Ashford, S.A., & Driscoll, N. (2011). "New automated point-cloud alignment for ground based lidar data of long coastal sections," Journal of Surveying Engineering, ASCE, 137(1), 14-25. http://dx.doi.org/10.1061/(ASCE)SU.1943-5428.0000030

Olsen, M.J., Johnstone, E., Driscoll, N., Ashford, S.A., & Kuester, F., (2009). "Terrestrial laser scanning of extended cliff sections in dynamic environments: a parameter analysis," Journal of Surveying Engineering, ASCE, 135(4), 161-169. http://dx.doi.org/10.1061/(ASCE)0733-9453(2009)135:4(161)

Olsen, M.J.; Roe, G.V.; Glennie, C.; Persi, F.; Reedy, M.; Hurwitz, D.; Williams, K.; Tuss, H.;, Squellati, A.; Knodler, M. Guidelines for the Use of Mobile LiDAR in Transportation Applications; TRB NCHRP Final Report 748; Publisher: TRB Washington, DC, USA. 2013

Pantelidis, 2009

Pierson, L. A. (1991). Rockfall Hazard Rating System. Washington, DC: Federal Highway Administration.

Pierson, 2012

Rabatel et al. 2008

Rosser et al. 2005, 2007

Silvia, E.P., and M. J. Olsen, "To Level or Not to Level: Laser Scanner Inclination Sensor Stability and Application," *J. Surv. Eng.*, Nov. 2011.

Trop, J. M., R. B. Cole, D. Sunderlin, C. Hults, and E. Todd, "Bedrock geology of the Glenn Highway from Anchorage to Sheep Mountain, Alaska," pp. 1–46, 2015.

Turner and Jayaprakas, 2012

Turner, A.K., Kemeny, J., Slob, S., and Hack R., (2006). "Evaluation and management of unstable rock slopes by 3-d laser scanning," Proceedings of IAEG2006.

Turner, D., Lucieer, A., de Jong, S. (2015). Time Series Analysis of Landslide Dynamics Using an Unmanned Aerial Vehicle (UAV). Remote Sensing. 7, 1736-1757, DOI:10.3390/rs70201736.

USGS (1999) Map Showing Inventory and Regional Susceptibility for Holocene Debris Flows, and Related Fast-Moving Landslides in the Conterminous United States, Misc. Field Studies Map 2329.

Wilkinson et al. (2016